THE ASTROPHYSICAL JOURNAL, 289:58–66, 1985 February 1

AN ANALYSIS OF OBSERVATIONS OF THE STREAMING VELOCITIES IN THE BULGE OF M31

P. TEUBEN,[1] EDWIN L. TURNER,[2] AND M. SCHWARZSCHILD
Princeton University Observatory
Received 1983 September 27; accepted 1984 August 13

ABSTRACT

McElroy has recently provided an extensive set of radial velocity measurements for the stellar mean motions in the bulge of M31. These velocities show a surprisingly bumpy pattern. It is frequently postulated that the absorption clouds in the bulge are the cause of these observed velocity bumps. If this postulate is correct, further improvements of the velocity measurements will be futile and their use as a dynamical diagnostic minimal.

To test this pessimistic hypothesis, we have analyzed the effects of the observed dust clouds on the velocity observations. Fortunately the observed clouds cannot be the main cause of the bumps in the observed velocities

Furthermore, a statistical analysis of the present velocity observations strongly suggests the existence of unidentified systematic errors which might explain the apparent bumps.

We conclude that the stellar mean motions in the bulge of M31 would have to be observed with an accuracy about twice as high as that of the present observations to be useful as a powerful tool for the study of the dynamics of this system and that even at this level of accuracy the existing clouds will not interfere with the dynamical interpretation of the observations.

Subject headings: galaxies: individual — galaxies: internal motions — stars: stellar dynamics

I. INTRODUCTION

The stellar motions in the bulge of the Andromeda Nebula have received much attention ever since the pioneering work of Babcock (1939). Recent observations by Pellet (1976), Peterson (1978), Schechter and Gunn (1979), Richstone and Shectman (1980), and McElroy (1983) provide fairly definitive data regarding the stellar velocity dispersion, which turns out to be the dominant kinematic feature. However, they do not provide a clear picture of the stellar mean motions (observed radial velocities) in the bulge. The mean motions are small compared with the velocity dispersion and hence are a secondary kinematic feature. Nevertheless, if clearly observable, they would be a powerful diagnostic tool for the stellar dynamics of the bulge.

The most recent and most extensive set of stellar radial velocity observations in the bulge of M31, that of McElroy (1983), presents an unexpectedly bumpy and irregular picture of the mean velocities across the bulge. These velocity deviations have been suspected to be caused by absorption clouds, of which a fair number are known to exist throughout the bulge of M31 (Hodge 1980; Gallagher and Hunter 1981; Kent 1983). A cloud will alter the observed velocity by reducing the contribution to the measured velocity from that segment of the line of sight located behind the cloud. Are the disturbing effects of the clouds sufficiently large to cause the irregularities in the observed velocities? To answer this question is the aim of this paper.

The unfortunately lengthy analysis required to answer this simple question is detailed in §§ II–V. A quite independent statistical analysis of the velocity observations is described in § VI. Its results corroborate those of the main analysis.

This discussion is aimed solely at the bulge of M31, not at its nucleus or at its disk. To minimize complications that might arise from the superposition of light from the disk onto the bulge light (McElroy 1983), only those velocity observations are here considered which refer to points in an elliptical area centered on the bulge with a semimajor axis of 2'.5 and a semiminor axis of 2'.0. Similarly, to avoid interference by the light of the nucleus, observations within 0'.5 of the center have been excluded. The area thus restricted is well covered by McElroy's velocity observations.

II. INTENSITY AND VELOCITY MODEL

A model for the mean velocity as a function of position within the bulge of M31 is required to assess the effects of absorption clouds on the velocity observations. Since an observed velocity corresponds to an intensity-weighted integration along the line of sight, the intensity of starlight emitted within the bulge also has to be modeled. The required models do not need to have high accuracy and have to cover reasonably well only our restricted area. The perfection of a King or a de Vaucouleurs model is not required, nor does the velocity model need to have a detailed dynamical base. It is, however, of practical advantage if the models are of such simplicity that the required integrals can be carried out analytically.

We adopt axisymmetric models both for the intensity and for the mean velocity. This is not to say that a triaxial figure and the corresponding dynamics might not be more correct for the bulge of M31 (Lindblad 1956; Stark 1977). But an axisymmetric model should suffice to bring out the irregularities here investigated. The effects of triaxiality are discussed briefly in § VII.

For the inclination of the rotation axis to the line of sight we adopt $i = 78°$ (Schmidt 1957; de Vaucouleurs 1958). This inclination was determined for the disk of M31 but will here be accepted for the bulge. For the position angle of the major axis

[1] On leave from the Kapteyn Laboratorium, Groningen University.
[2] Alfred P. Sloan Research Fellow.

of the bulge over the extent of our restricted area we adopt P.A. = 50° (Lindblad 1956; Hodge and Kennicutt 1982; Kent 1983). In contrast, the major axis of the disk lies at P.A. = 38°. Finally, we adopt for the observed axis ratio of the bulge in our restricted area the average value $(c/a)_{obs} = 0.80$ (Kent 1983).

For the intensity model we take the simple form

$$\rho = \frac{\rho_0}{1 + m^2},$$

where

$$m^2 = \frac{x^2 + y^2}{a^2} + \frac{z^2}{c^2}. \tag{1}$$

The core radius, a, and the intrinsic axis ratio, c/a, are to be derived by fitting the model to the photometric data.

Let us denote the coordinates in the plane of the sky by ξ and ζ, with ξ along the major axis of the bulge, and the coordinate along the line of sight by η. These coordinates are related to those along the principal axes of the bulge by the usual transformation

$$\begin{aligned} \xi &= x, \\ \eta &= y \sin i + z \cos i, \\ \zeta &= -y \cos i + z \sin i. \end{aligned} \tag{2}$$

The projected surface brightness can now be readily obtained by integration of equation (1) along the line of sight (see Appendix),

$$\mu(\xi, \zeta) = \int_{-\infty}^{+\infty} \rho d\eta = \frac{\mu_0}{(1 + m_{obs}^2)^{1/2}}, \tag{3}$$

where

$$\mu_0 = \pi\rho_0 \left(\frac{\sin^2 i}{a^2} + \frac{\cos^2 i}{c^2} \right)^{-1/2} \tag{4}$$

and

$$m_{obs}^2 = \frac{\xi^2}{a^2} + \frac{\zeta^2}{a^2 \cos^2 i + c^2 \sin^2 i}. \tag{5}$$

Hence the observed axis ratio will be (cf. Contopoulos 1956)

$$(c/a)_{obs}^2 = \cos^2 i + (c/a)^2 \sin^2 i. \tag{6}$$

Our adopted value for the observed axis ratio gives then, for the intrinsic axis ratio, $c/a = 0.790$. Note also that, according to equation (5), the surface brightness has the same core radius as the intensity model of equation (1). This core radius can be determined by fitting equation (3) to the observed brightness profile along the apparent major axis (Kent 1983, Table 2). This fit, limited to our restricted area of $r = 0'.5$–$2'.5$, yields $a = 0'.48$.

Next we adopt a simple velocity model. We take the mean streaming velocity inside the bulge to be purely rotational and constant on cylinders. For the rotation velocity, v_{rot}, as a function of the distance from the axis, R, we accept the simplest possible form, namely, a linear rise out to a turnover radius, R_0, and a constant value from there on out, i.e.,

$$\begin{aligned} v_{rot} &= R\left(\frac{v_0}{R_0}\right) \quad \text{for} \quad R < R_0 \\ &= v_0 \quad \text{for} \quad R \geq R_0. \end{aligned} \tag{7}$$

The observed velocity at a given point in the sky will be the intensity-weighted velocity, integrated along the line of sight (McElroy 1983),

$$V(\xi, \zeta) = \int_{-\infty}^{+\infty} \rho v d\eta \Big/ \int_{-\infty}^{+\infty} \rho d\eta, \tag{8}$$

where v within the integral denotes the radial velocity as a function of position along the line of sight. The simplicity of our model has the advantageous consequence that the integral in equation (8) can be expressed analytically, as is detailed in the Appendix.

We still have to determine the two parameters in equation (7) for the velocity model, v_0 and R_0, by fitting the radial velocity derived from the model through equation (8) to the observed radial velocities (McElroy 1983) along or near the major axis. This fitting procedure is made easy by the fact that equation (8) together with equation (7) gives a maximum value, V_{mx}, for the observed radial velocity $V(\xi, \zeta)$ along the major axis, $\zeta = 0$, at distances ξ from the projected rotation axis that are larger than the turnover radius R_0 and substantially larger than the core radius a. Here equation (8) becomes scale-free and tends toward a limit (see Appendix, eq. [A15]). For our values one finds

$$V_{mx} = 0.6440 v_0 \sin i. \tag{9}$$

The numerical coefficient in this equation is substantially less than 1 because the integration along the line of sight gives appreciable weight to places away from the equatorial plane where the rotation velocity is tilted away from the line of sight.

McElroy's (1983) data for the outer portions of our restricted area near the major axis suggest $V_{mx} \sim 40$ km s^{-1}. This gives, according to equation (9), $v_0 = 63.5$ km s^{-1}. Finally, McElroy's data for points nearer to the projected rotation axis indicate a tolerable fit for $R_0/a = 2 \pm 0.25$, or $R_0 = 0'.96$.

With all the parameters of our intensity and velocity models thus fixed, we can compute the radial velocity $V(\xi, \zeta)$ to be expected from the model at any point on the sky with the help of equation (8), or its detailed forms discussed in the Appendix. Such computations have been carried out for the 216 points in our restricted area for which McElroy (1983) gives observed velocities. The resulting residual velocities (observed minus model) are displayed in Figure 1. They have a surprisingly patchy appearance, with a fair fraction of them exceeding 15 km s^{-1}, a problem which has already been noted and addressed by McElroy.

In the next three sections we will discuss the possibility that these residuals are caused by absorption clouds modifying the line-of-sight integrations. Our discussion will thus be an extension of the initial discussion of this topic by McElroy (1983).

III. EFFECT OF A CLOUD ON OBSERVED VELOCITY

The integration along the line of sight which according to equation (8) gives the observed velocity has to be modified to study the effect of a cloud located on the line of sight. If we denote the position of the cloud by η_c and its optical depth by t_c, equation (8) becomes

$$V_c(\xi, \zeta) = \frac{e^{-t_c} \int_{-\infty}^{\eta_c} \rho v d\eta + \int_{\eta_c}^{\infty} \rho v d\eta}{e^{-t_c} \int_{-\infty}^{\eta_c} \rho d\eta + \int_{\eta_c}^{\infty} \rho d\eta}. \tag{10}$$

This equation takes properly into account the absorption effect of the cloud, but it does not include the scattering, or reflection, effect. The neglect of scattering will generally not cause a

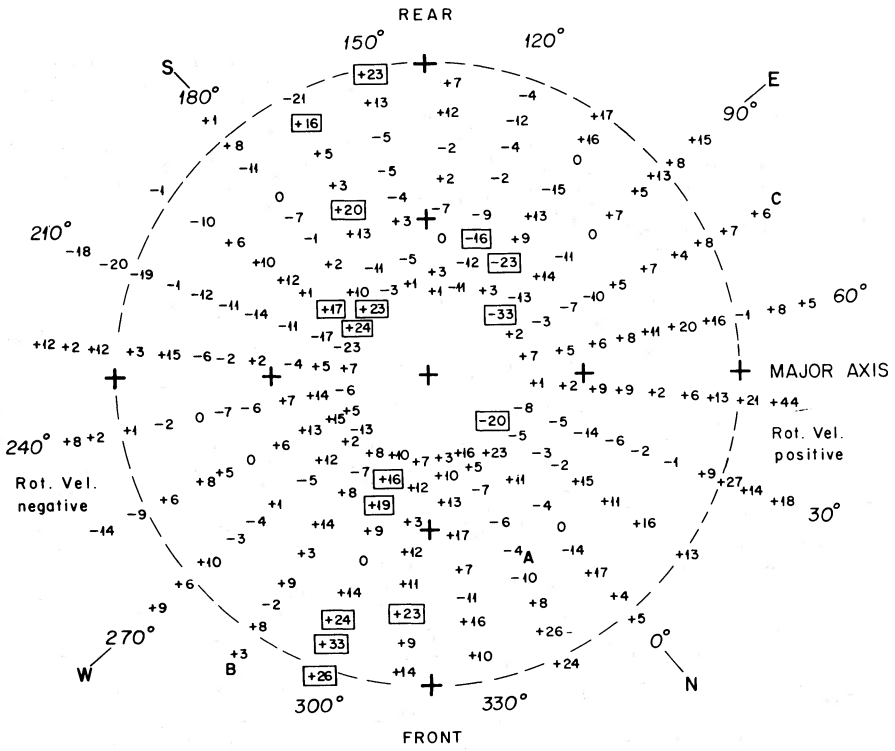

FIG. 1.—Velocity residuals (observed minus model), in km s^{-1}, in the bulge of M31. The coordinate marks are spaced 1′ apart. Boxes indicate residuals which exceed 15 km s^{-1} and which have a sign designating deficiency in rotation velocity (see text). Letters *A*, *B*, and *C* give the locations of the clouds listed in Table 1. The circle has a radius of 2′.

noticeable velocity error for a cloud located in the front section of the line of sight. But it may cause a somewhat larger error for a cloud in the rear section, since such a cloud will scatter additional light from the stars in front of it into the line of sight, and this scattered light will have a modified Doppler shift. Luckily such backward scattering is weak. We will proceed by using equation (10) as it stands, keeping in mind the possibility of errors for clouds located toward the back.

The effect of a cloud on the observed velocity may best be brought out by defining the rotation excess

$$\Delta V = V_c(\xi, \zeta) - V(\xi, \zeta) , \qquad (11)$$

where V_c is determined from equation (10) including the cloud and V is determined from equation (8) for the same line of sight but without the cloud. The qualitative behavior of this rotation excess in its dependence on the location of the cloud can be understood as follows.

Along a line of sight the rotational mean velocity will have a high component parallel to the line of sight in the middle section where the rotation direction comes closest to the line-of-sight direction. In contrast, the front and rear sections will contribute less to the observed radial velocity because in these sections the rotation direction is more nearly perpendicular to the line of sight. Accordingly a cloud located toward the rear will reduce the low-velocity contribution of the rear section and thus produce a positive rotation excess. This positive excess will appear in Figure 1 as a positive residual in the right half, where the rotation velocity is positive, and as a negative residual in the left half, where the rotation velocity is negative. In contrast, a cloud located toward the front will reduce not only the contribution of the rear section but also the high-velocity and high-intensity contribution of the middle section and thus produce a negative rotation excess, which appears in Figure 1 as a negative residual on the right and a positive residual on the left. On each line of sight there is a middle position at which a cloud produces zero rotation excess.

The amount of rotation excess produced by a cloud depends on its opaqueness, particularly for clouds in forward positions. A very opaque cloud in a far forward location can have so large a negative rotation excess as to reduce the observed velocity to a small fraction of its cloudless value. But such a cloud would be photometrically outstanding, since it would greatly dim the surface brightness. Thus, to assess the possible effects of clouds on the observed velocities quantitatively, it is of great value to have photometric data in addition to the velocity data. Here we have the great advantage of having the recent photometry of Kent (1983) for the bulge of M31.

To exploit the photometric data we have to introduce the effect of a cloud on the line of sight into equation (3) for the surface brightness. We may express the effect of the cloud by the magnitude difference between the surface brightness dimmed by the cloud and a corresponding cloudless surface brightness. Thus we get for the extinction

$$\Delta m = -2.5 \log \left(\frac{e^{-t_c} \int_{-\infty}^{\eta_c} \rho d\eta + \int_{\eta_c}^{\infty} \rho d\eta}{\int_{-\infty}^{+\infty} \rho d\eta} \right) . \qquad (12)$$

Here we have again neglected scattering. For clouds in forward positions this again will probably not cause noticeable errors, but for clouds in backward positions it may.

Equations (10), (11), and (12) permit us to compute the rotation excess and the extinction for any cloud, specified by its location η_c and its optical thickness t_c, at any point (ξ, ζ) in our restricted area in the bulge of M31. Figure 2 shows the results

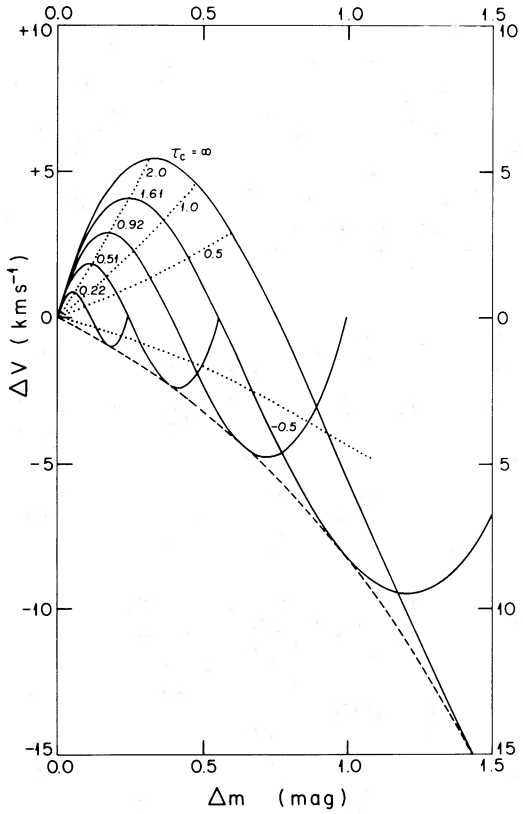

FIG. 2.—Rotation excess Δv vs. extinction Δm for clouds projected onto the apparent major axis ($\zeta = 0$) at $\xi = 2'$. The solid curves are labeled by values of the optical depth. The dotted curves are labeled by values of the line-of-sight coordinate η_c of the cloud in minutes of arc. The dashed curve gives the lower envelope.

of such computations for a specific point on the major axis ($\zeta = 0$) 2′ from the center ($\xi = 2$). Here the expected rotation excess, ΔV, has been plotted against the extinction, Δm. Any one of the solid curves represents a sequence of clouds equal in optical depth but differing in their location, η_c, along the line of sight, low Δm being caused by clouds toward the rear and higher Δm by near-front clouds. Each such curve shows positive ΔV for clouds in the rear section and negative ΔV for clouds in the front section.

All the curves in Figure 2 fall within an area restrained by two envelopes. The upper envelope limits the positive ΔV and corresponds to totally opaque clouds located along the rear half of the line of sight. The lower envelope (dashed curve in Fig. 2) limits the negative ΔV and corresponds to a sequence of clouds varying in optical depth but all located on the front section of the line of sight. Our neglect of scattering will have little effect on the lower envelope but may have noticeably affected the upper envelope.

If a cloud is located at the position ($\xi = 2$, $\zeta = 0$) for which Figure 2 was computed, and if the extinction Δm of the cloud is photometrically determined, then one can read from Figure 2 both the positive and the negative extremes for ΔV, to be compared with the observed ΔV. It remains to extend these results derived from the model to other positions (ξ, ζ) in our restricted area of the bulge.

Computations have been carried out for points farther out along the major axis ($\zeta = 0$). The resulting graphs turned out to be practically identical with Figure 2. This was to be expected, because our model is nearly scale-free for large ξ. Even at $\xi = 1$ on the major axis the resulting graph does not differ noticeably from Figure 2.

For points not located on the major axis, calculations have been carried out for several points, all at $\xi = 2$ but with varying values of ζ/ξ. The results are shown in Figure 3, in terms of the two envelopes for each position. The curves for the lower envelopes show that the extreme negative rotation excesses are reached for $\zeta/\xi \sim -2$ as long as $\Delta m \lesssim 1$. The curves for the upper envelopes show that the extreme positive rotation excesses are reached for $\zeta/\xi \sim +2$ and that the range of extinction over which positive rotation excesses occur extends to a maximum of $\Delta m = 0.97$ for $\zeta/\xi \to \infty$.

Further calculations for points off the major axis have shown that for practical purposes Figure 3 can be applied for all points with $\xi \gtrsim R_0 \sim 1$, again not surprising in view of the nearly scale-free character of our model at sufficiently large ξ. Finally, computations for points located nearer to the rotation axis, i.e., $\xi < 1$, show that the resulting envelopes are practically the same as those in Figure 3, except that now the scale for the rotation excess is reduced, with the reduction factor varying approximately linearly with ξ from $\xi = 0$ to $\xi = 1$. This result might have been expected, since for $\xi < 1$ the main contribution to the observed velocity comes from $R < R_0$, where our model rotation curve, equation (7), is linear.

Thus we end with the following recipe for deriving the extreme values of the rotation excess permitted by our model for a cloud which is located at (ξ, ζ) in our restricted area of the bulge of M31 and for which the extinction Δm has been mea-

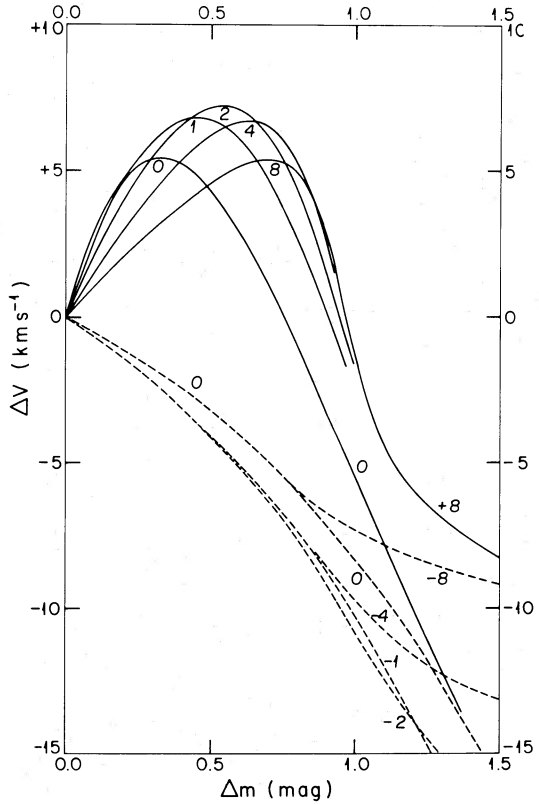

FIG. 3.—Upper envelopes (*solid curves*) and lower envelopes (*dashed curves*) in the Δm-Δv diagram for clouds projected onto various positions on the sky with $\xi = 2'$. The curves are labeled with values of ζ/ξ.

sured. (1) Enter Figure 3 at the observed Δm value. (2) Read the ΔV values from the upper and lower envelope curves labeled with the ζ/ξ value corresponding to the cloud position. (3) Accept these values as extrema if $\xi \geq 1$. If $\xi < 1$, multiply the values of ΔV by ξ and then accept them as extrema.

IV. PHOTOMETRY OF CLOUDS

The preceding discussion makes it clear that tight limits on the velocity effects, ΔV, of absorption clouds can be established only if limits on their photometric effect, Δm, can be obtained. This is particularly true for a cloud located in the front section of the line of sight, where it could significantly reduce the apparent rotation velocity if it were dark enough.

Photometric data for the clouds in the bulge of M31 have recently been given by Gallagher and Hunter (1981) and by Kent (1983). Both studies give for the photometric effect of each cloud in the blue or green $\Delta m \lesssim 0.1$ mag. In neither case, however, is this value meant as a strict upper limit. Kent (1983) mentions the existence of a few darker clouds, while Gallagher and Hunter (1981) concentrate on clouds of rather small lateral extent, leaving open the possibility of somewhat larger clouds or cloud complexes with stronger photometric effects.

The opportunity for deriving anew the photometric limit here required was afforded us by Dr. Kent, who kindly sent us the digital data from his two main CCD exposures, one in the green (4690 Å) and the other in the red (6500 Å). These exposures are centered on the nucleus of M31 and cover most of our restricted area.

Each of these two intensity arrays reduced by averaging four by four pixels was fitted by the approximate model described in § II, and digital maps for the magnitude residuals were prepared. The large-scale gradients in these maps which are caused by the imperfections of the model are sufficiently shallow to leave the stronger clouds quite outstanding. Following Kent's precedent (1983, particularly his Fig. 1), a third digital map was prepared which shows the array of color indices—without any need for a model. As Kent had emphasized, this map shows the stronger clouds very well indeed.

Table 1 gives the photometric results for the three most outstanding clouds in our restricted area of the bulge of M31, again excluding the nuclear region within 0.5 from the center. The photometric data are estimated to have an uncertainty of about 0.02 mag, most of which is contributed by the uncertainty in the choice of the "cloudless" comparison regions. The color excesses listed in the last line were taken from the color map, which presumably gives somewhat more accurate results than could have been obtained by simply differencing Δm_g and Δm_r.

Similar data, although more extensive in wavelength coverage, have been obtained by Elmegreen (1980) for clouds in several other galaxies and have been analyzed by her in detail. This analysis includes two effects here relevant for clouds well embedded inside the stellar system. Such a cloud, first, will absorb and redden only that fraction of the starlight arising from behind it (an effect taken into account by the equations of § III), and, second, it will scatter, without reddening, additional light into the line of sight from stars in front of it (an effect neglected in § III). Both effects decrease the observed absorption, Δm_g, and the relative reddening, Δ(C.I.)/Δm_g, compared with an identical cloud positioned in front of all stars. Elmegreen's specific computations of these effects cannot be applied here because they refer to several cloud types all more opaque than the clouds here considered. Nevertheless, the data given in Table 1 can be discussed with due regard to these two effects, as follows.

TABLE 1

PHOTOMETRIC DATA FOR THREE CLOUDS IN THE BULGE OF M31

Quantity Measured	Cloud A	Cloud B	Cloud C
E-W coordinate (arcmin)	W 0.3	W 2.2	E 2.4
N-S coordinate (arcmin)	N 1.3	N 0.6	N 0.6
Δm_g (mag)	0.27	0.12	0.09
Δm_r (mag)	0.14	0.08	0.06
Δ(C.I.) (mag)	0.12	0.06	0.04

Of the three clouds listed in Table 1, cloud A is the darkest. It is No. 395 in the catalog of Hodge (1980) and has also been included in the study by Gallagher and Hunter (1981). It shows a relative reddening of Δ(C.I.)/$\Delta m_g = 0.4$. The relative reddening of a separate cloud would be expected, from the compilation by Savage and Mathis (1979), to amount to $1/2.9 = 0.34$ for Kent's wavelength bands. The apparent discrepancy is within the uncertainty of the present data, but makes it unlikely that the true relative reddening of this cloud is substantially less than the expected value. This then argues for a position of this cloud in front of most of the stars in the bulge. The same position is favored by the cloud's apparent location northwest of the apparent major axis of the bulge, which places it toward the front side of the bulge if one assumes that it lies on or near the equatorial plane. Thus, following both lines of evidence, one may accept for this cloud a near-front position and accordingly take the data for it in Table 1 at their face value. We then conclude that for this cloud Δm in the blue (where the radial velocities are measured) likely is not larger than 0.3 mag.

Similar arguments hold for cloud B of Table 1. Its photometric effects are much weaker than those of cloud A, but its relative reddening is again strong, Δ(C.I.)/$\Delta m_g = 0.5$, though more uncertain. This again suggests a front position, which is also suggested by its apparent location at the front edge of the area here studied. Thus one may conclude for this cloud, as for cloud A, that the two complicating effects discussed earlier do not play a significant role, so that one can take the photometric values as they stand. Accordingly it appears likely that the Δm in the blue for cloud B is about 0.15 mag.

Cloud C, in spite of being one of the most outstanding clouds in the area of the bulge here investigated, is photometrically much weaker than cloud A. Nevertheless, it is clearly discernible on all three maps. Its apparent location at the rear edge of our restricted area suggests that its actual location, if it is near the equatorial plane, should be in the rear portion of the bulge. On the other hand, the small but distinct reddening effect, Δ(C.I.), of this cloud does not permit a position too far back in the bulge. One can very roughly model this cloud by adopting for it a position such that two-thirds of the bulge stars along the line of sight lie in front of the cloud, by taking for it an optical depth of 1.0 in the green, and by assuming that the scattered light is approximately equal to 20% of the light of the stars in front of the cloud. This rough model reproduces the observed value of Δm_g but gives for Δ(C.I.) only 0.02 mag, the minimum value necessary to make this cloud appear as outstanding as it is on the color map. Since in the analysis of § III the scattered light was neglected, it is here necessary to note the effective value of Δm_g which the cloud model would produce without the scattering. This value

turns out to be 0.25 mag, i.e., substantially larger than the value actually observed. In the blue range, relevant for the velocity measurements, one finds $\Delta m \sim 0.3$, i.e., about the same value as for cloud A in spite of the substantially higher opacity of cloud C.

The discussion of cloud C raises the question of whether there might be a number of clouds in the rear portion of the bulge of M31 located so that the light gained by scattering just about compensates for the light lost by absorption. If each such cloud furthermore is sufficiently opaque so as to transmit little reddened light, it might not be detected in either the Δm or the Δ(C.I.) maps. But if such opaque clouds exist in the rear half of the bulge of M31, some similar clouds should also exist in the front half. These would be outstandingly observable but are absent.

All together, then, we conclude that we may adopt, in connection with the analysis of § III, a value of 0.3 as an upper limit for Δm for the clouds in the bulge of M31.

V. RESULTS FOR CLOUD EFFECTS ON VELOCITIES

Let us start with a qualitative argument. The three photometrically outstanding clouds discussed in § IV are marked in Figure 1 with their designations A, B, and C. The figure shows that the observed velocity residuals nearest to the three cloud locations are among the smaller ones of all the residuals. This lack of correlation already suggests that clouds are not the main cause for the velocity residuals. We should reemphasize that here we are concerned only with our restricted area. For some points outside our area McElroy has already pointed out cases of coincidence between clouds and large velocity residuals, but not in our restricted area.

Let us now turn to the main quantitative argument. With the tight limit on the cloud extinction derived in § IV, namely, $\Delta m \leq 0.3$ mag, we can now set a tight limit on the rotation excess ΔV produced by a cloud, regardless of its position. If we enter Figure 3 with the extinction limit, we find an extreme value for positive rotation excesses of 6 km s^{-1} and an extreme value for negative rotation excesses of 2.3 km s^{-1}. We should view the positive limit with caution, since it could be noticeably affected by our neglect of scattering. The true value might be higher. On the other hand, the negative limit should not be noticeably affected by this effect. Accordingly, we will concentrate on this limit.

The limit of 2.3 km s^{-1} for negative rotation excesses deduced from the model should be compared with those observed velocity residuals shown in Figure 1 which have signs corresponding to negative velocity excesses (negative in the right half and positive in the left half). There are 109 such residuals, out of a total of 216. Of these, 16 have values in excess of 15 km s^{-1}. They are shown in boxes in Figure 1. These large observed velocity residuals with a sign corresponding to negative rotation excesses are the ones which violate the limit of 2.3 km s^{-1} deduced from the model by so large a factor that they could not plausibly be explained as mainly effects of clouds, even if a more elaborate and more carefully adjusted model were employed. Our model gives a limit of less than 6% of the maximum observed rotation velocity on the major axis, while the average absolute value of the 16 large residuals amounts to about 50% of this maximum.

We should add a comment regarding the residuals opposite in sign to those just discussed. There are 20 residuals exceeding 15 km s^{-1} with a sign corresponding to positive rotation excess. The contrast of these residuals to the corresponding model limit of 6 km s^{-1} is not so striking if one remembers that this limit is somewhat uncertain because of our neglect of scattering. But one may argue that if the residuals implying negative rotation excesses are not caused by clouds, then the majority of the residuals of the opposite sign likely are not caused by clouds either.

We conclude that the main cause for the observed velocity residuals in our restricted area in the bulge of M31 is nearly certainly not to be found in the effects of clouds.

VI. STATISTICS OF VELOCITY RESIDUALS

In § II above, a simple model for rotational streaming velocities was fitted to McElroy's (1983) M31 velocity data. In this section we will examine the statistical properties of the velocity residuals generated by comparing the data with the model. Our object will be to distinguish random independent measuring errors, systematic velocity errors, and real departures of the M31 velocity field from our model, all of which contribute to the residuals. We shall be particularly interested in spatially correlated, large-amplitude residuals which could be indicative of greater dynamical complexity. In the following analysis we shall restrict our attention to the velocity residuals in the circular annulus constrained by $0'.5 < r < 2'.0$, giving a total of 186 measured points. This region is indicated by a dashed circle in Figure 1.

As a first step we compare the residuals with McElroy's (1983) velocity error estimates (which are based on a Fourier quotient analysis of his data) by examining the distribution of the ratio of residual to estimated error. If the residuals were entirely the result of random measuring errors which were accurately characterized by the error estimates, this distribution would be a Gaussian with a mean of zero and a variance of unity. In fact, the variance is 1.56, and more than 6% of the residuals exceed the estimated 3 σ level. This strongly suggests that either the real errors are $\sim$50% greater than the estimated ones or the residuals are not entirely due to random measuring errors.

In order to distinguish these two possibilities, we examine the correlation of neighboring velocity residuals, taking care to separate pairs of velocities measured along the same slit position angle (generally on the same spectrogram) from those with differing position angle. The former could be subject to common systematic errors, while the latter probably would not be. We define a correlation variable K to be the product of two velocity residuals and consider the K-distributions for various pairings of the McElroy velocity measurements. The distributions are compared by their means and dispersions and by a Kolmogorov-Smirnov (hereafter KS) test (Lehmann 1975). The mean separation, s, between pairs of points and its dispersion are also calculated, in order to determine the approximate angular scale of any positional correlation in the residuals.

Four K-distributions, including one control case, have been calculated and compared. For the control case we have paired each point with a point at a position angle 165° smaller than the chosen point but with the most nearly equal radial coordinate. In effect, this produces a distant (and hence presumably uncorrelated) velocity residual measured on a different spectrogram but at approximately the same surface brightness as the chosen point. A 180° shift would have brought us back to the same spectrogram in many cases. Any K-distributions which are indistinguishable from this control, which we label case C, are considered uncorrelated. Our only internal check on the actual lack of correlation in case C is that its mean K

should be zero within the measuring errors. The second K-distribution, which we call case NR (near, radial), is generated by pairing each point with its nearest neighbor at the same position angle, which is generally its absolutely nearest neighbor on the residual map. A third K-distribution, called case A (azimuthal), is constructed by pairing each point with its nearest neighbor with a position angle 15° greater than its own. Finally, a fourth distribution, called case R (radial) is calculated by again pairing each point with a point at the same position angle, but this time with the constraint that the point be as nearly as possible at the same angular distance as in case A; this means that we are correlating points at the same slit position with separations as large as those between slit positions.

Table 2 gives the results of our statistical analysis for each of these four cases. The first column gives a letter code specifying the particular pairing of residuals as described in the previous paragraph. The second and third columns give the mean (with its associated uncertainty) and dispersion of the angular separation s of the paired points, respectively. Columns (4) and (5) give the same statistics for the K-variable itself. Finally, column (6) gives the KS probability, that is, the probability that the particular K-distribution would be as different as it is from the case C distribution of K if it was in fact drawn from the same parent population. Small values of this last parameter are taken to indicate correlated velocity residuals.

The results given in Table 2 are clear and reasonably easy to interpret. First of all, we note that the mean K-value in case C is consistent with zero, which supports our expectation that these widely separated residuals are uncorrelated. Second, case NR shows that adjoining velocity residuals at the same slit position angle are strongly correlated. This is no surprise, since such correlations are evident to the eye in Figure 1 and indeed are clearly visible as bumps in the rotation curves plotted in McElroy's (1983) original paper. Third, the results for case A show that there is no significant correlation of residuals from one slit position angle to the next. This could mean that the case NR correlations are due to systematic velocity errors, or it could be due to the increased angular scale of the pairings from case NR to case A. Finally, case R can be used to rule out this second possible explanation by showing that for constant position angle the correlations are only slightly reduced in significance for angular separations just as large as those between adjacent slit position angles (case A). In short, velocity residuals show correlations where they are typically due to measurements on the same spectrogram but not otherwise.

Our conclusions from this analysis are that the velocity model presented in § II adequately reproduces all of the real features in the velocity field of M31's nucleus to an accuracy of ~ 10 km s^{-1}, and that the deviations from this model in McElroy's (1983) data (the bumps and asymmetries of his measured rotation curves) are probably due to small systematic measuring errors with amplitudes comparable to his (rather small) random errors. No real velocity bumps in the bulge of M31 are likely to have amplitudes much larger than 10 km s^{-1}, since, if they did, they should have been detected by McElroy.

TABLE 2

STATISTICS OF VELOCITY RESIDUALS

	s (arcsec)		K (km^2 s^{-2})		
CASE	Mean[a]	Dispersion	Mean[a]	Dispersion	P_{KS}
C	136(4)	55	3.6(11)	147	1.0
NR	10.8(0.1)	1.7	59(10)	143	$<10^{-4}$
A	19.3(0.5)	6.7	13(10)	134	0.7
R	19.1(0.5)	7.0	42(9)	125	10^{-4}

[a] Uncertainties in parentheses.

VII. SPECULATIONS ON THE DYNAMICS OF THE BULGE

The negative results of the preceding sections bring up the questions of, first, what dynamical phenomena might exist in the bulge of M31 that could produce a more complicated velocity pattern than the simple one here modeled, and, second, what would be the required observational accuracy if these phenomena were to be investigated. We will discuss here, in a speculative manner, only one such phenomenon, namely, that caused by a triaxial rather than an axisymmetric figure for the bulge.

Lindblad (1956) has suggested a triaxial figure to explain the 12° tilt of the apparent major axis of the bulge to that of the disk. A further discussion of this possibility has been presented by Stark (1977). The internal dynamics of a triaxial stellar system depends critically on its figure rotation speed. Fast-rotating bars have been investigated with the help of N-body calculations (e.g., Miller and Smith 1979; Hohl and Zang 1979; Sellwood 1981). Slow-rotating triaxial figures have been investigated by numerical procedures for the derivation of equilibrium models (Schwarzschild 1982).

The bulge of M31 probably belongs to the slow figure rotation class because of its low net rotation. Accordingly we use Schwarzschild's (1982, Figs. 8 and 9) models as a guide for the deviations of the velocity pattern in a triaxial figure from that of a simple axisymmetrical model. The numerical models indicate that in favorable cases the observable deviations may amount to 10% of the velocity dispersion but will in general be somewhat less. We conclude that triaxiality may cause diagnostic effects in the observable velocities of the order of 10 km s^{-1}.

For the models referred to above, the velocity data are given only for viewing directions parallel to the long and intermediate axes. But for streaming motions in a triaxial figure, when viewed from a direction not aligned with a principal axis, another perspective velocity distortion appears, namely the S-distortion along the apparent minor axis (cf. Miller and Smith 1979, Fig. 10). The distortion is well known for gas motions in barred galaxies (e.g., Sancisi, Allen, and Sullivan 1979) and has recently been found by Kormendy (1983) for stellar motions in NGC 936, with a maximum value of about 20 km s^{-1}. However, NGC 936 is a fast-rotating barred galaxy. Accordingly, in the bulge of M31 a much weaker S-distortion is expected. Thus the direct effects discussed above seem likely to be the main ones.

What, then, is the accuracy required to uncover the effects of triaxiality by velocity measurements? We estimate that an accuracy corresponding to an rms error, including intrinsic and extrinsic sources, of ± 5 km s^{-1} should suffice. The estimated effect of triaxiality is only twice as large as this rms value. But the triaxiality effect is of fairly large scale in the sky plane and might be established by combining measurements from various points. We recognize that this accuracy requirement is very high.

VIII. SUMMARY

We have arrived at two conclusions. First, contrary to a common suspicion, the velocity residuals derived from

McElroy's (1983) extensive radial velocity observations in the inner bulge of M31 are not likely to be caused by the effects of absorption clouds. Second, the statistics of the velocity residuals suggest that they are caused mainly by systematic observational errors that are not accessible to the objective internal error analysis.

The accuracy of McElroy's (1983) observations is indicated by the small rms error of the velocity residuals. If one considers only those observations within our restricted area (2'.5 from the center on the major axis and 2' on the minor axis), this turns out to be ± 11 km s^{-1}, which amounts to only 3% of the 400 km s^{-1} width (FWHM) of the absorption lines. Even this accuracy does not suffice to address dynamical problems such as those mentioned in § VII.

However, a substantially higher accuracy has been obtained by McElroy on those position angles (45°, 135°, 225°, and 315°) where he had 4 m spectra available. On these position angles, and with the further restriction to $0'.5 < r < 1'.5$, where the surface brightness is high and fairly flat, one finds from the velocity residual an rms error of ± 6 km s^{-1}. If data of this accuracy or a little higher were available for all 24 of McElroy's position angles, even if only in the restricted range for r just mentioned, they might reveal dynamical effects such as those due to triaxiality, without any serious disturbances from the absorption clouds.

We gratefully acknowledge essential help in this work as follows. P. Schechter pointed out the main problem to us. D. McElroy, in addition to sending us a preprint of his paper, provided us with much further information. S. Kent sent us a tape containing the data from his two main CCD exposures. W. Sebok transferred these data into our departmental computer system. One of us (P. T.) is supported by the Netherlands Organization for the Advancement of Pure Research (ZWO); this support included funds for travel to Princeton. This research was supported by NSF grants AST78-23796 and AST82-16717.

APPENDIX

The geometry is defined in Figure 4, in which (x, y, z) is the coordinate system in which the density is constant on similar ellipsoids, and (ξ, ζ) are the projected sky coordinates, with η along the line of sight. The inclination of the galaxy, i, is defined as the angle between the rotation axis, z, and the line of sight. Furthermore, ξ is defined to lie along the (projected) major axis. The transformation is given by equation (2). In Figure 4 the integration path along the line of sight is drawn as the heavy line.

Integrations along the line of sight, η, turn out to be easier when we use the transformation

$$l = \eta - \eta_0 = \eta - \frac{\zeta}{\tan i} . \tag{A1}$$

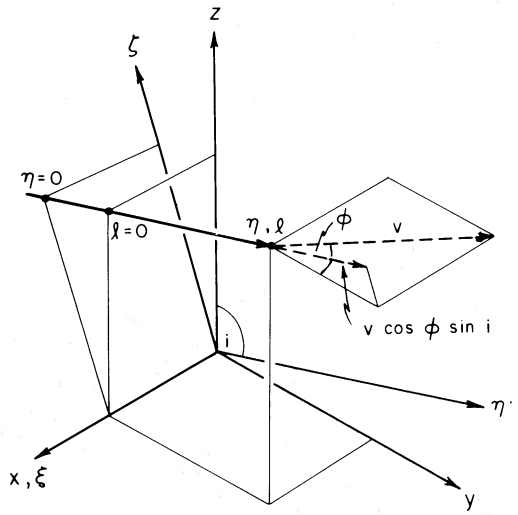

FIG. 4.—Coordinates and velocities in the bulge of M31: x, y, z are the principal axes of the bulge; ξ, ζ are the coordinates in the plane of the sky; η or l is the coordinate along the line of sight; v is the rotational velocity; and $v \cos \phi \sin i$ is the velocity component along the line of sight.

The line l is thus given in vector representation as

$$l_i = \begin{pmatrix} x \\ y \\ z \end{pmatrix} = \begin{pmatrix} \xi \\ \eta \sin i - \zeta \cos i \\ \eta \cos i + \zeta \sin i \end{pmatrix} = \begin{pmatrix} \xi \\ l \sin i \\ l \cos i + \zeta / \sin i \end{pmatrix} . \tag{A2}$$

To find the surface density according to equation (1), one needs

$$1 + m^2 = 1 + \frac{x^2 + y^2}{a^2} + \frac{z^2}{c^2} \equiv Al^2 + Bl + C ,$$

in which

$$A = \frac{\sin^2 i}{a^2} + \frac{\cos^2 i}{c^2} ,$$

$$B = \frac{2\zeta}{c^2 \tan i} ,$$

$$C = \frac{\xi^2}{a^2} + \frac{\zeta^2}{c^2 \sin^2 i} + 1 . \tag{A3}$$

A contribution from l_1 to l_2 to the surface density at (ξ, ζ) is thus given by

$$\rho_0 \int_{l_1}^{l_2} \frac{dl}{Al^2 + Bl + C} . \tag{A4}$$

This is a standard integral (e.g., Gradshteyn and Ryzhik 1965, No. 2.172). In the case of a cloudless path of integration with $l_{1,2} = \pm \infty$, the integral yields

$$\mu(\xi, \zeta) = \frac{2\pi\rho_0}{(4AC - B^2)^{1/2}} , \tag{A5}$$

which is given in equation (3).

To find the contribution from l_1 to l_2 to the velocity integral, equation (8), we need to multiply the integrand in expression (A4) by the radial velocity $v(l)$. Since velocities transform also

according to equation (2), we write, from Figure 4,

$$v(l) = v_{\rm rot}(R)\sin i\cos\phi$$
$$= [v_{\rm rot}(R)\sin i]\frac{\xi}{(\xi^2 + l^2\sin^2 i)^{1/2}}. \quad \text{(A6a)}$$

But since

$$v_{\rm rot}(R) = v_0 \quad \text{if} \quad R = (\xi^2 + l^2\sin^2 i)^{1/2} > R_0$$
$$= (v_0/R_0)R \quad \text{if} \quad R = (\xi^2 + l^2\sin^2 i)^{1/2} < R_0,$$

we obtain

$$v(l) = (v_0\sin i)\frac{\xi}{(\xi^2 + l^2\sin^2 i)^{1/2}}, \qquad R > R_0$$
$$= (v_0\sin i)\frac{\xi}{R_0}, \qquad R < R_0. \quad \text{(A6b)}$$

Since, for $R < R_0$, $v(l)$ does not depend on l, this contribution to the integral (8) is of the same standard form as (A4):

$$(\rho_0 v_0\sin i)\frac{\xi}{R_0}\int_{l_1}^{l_2}\frac{dl}{Al^2 + Bl + C}. \quad \text{(A7)}$$

For $R > R_0$ we write the contribution as

$$\rho_0 v_0\frac{\xi}{A}\int_{l_1}^{l_2}\frac{dl}{(\alpha + \beta l + l^2)(a_1 + l^2)^{1/2}}, \quad \text{(A8)}$$

with

$$\alpha = C/A, \qquad \beta = B/A, \qquad a_1 = \xi^2/\sin^2 i.$$

This integral is also of "standard" form, according to Gradshteyn and Ryzhik (1965, No. 2.252), and can be handled as follows: In the case $\beta \neq 0$ we substitute

$$l = \mathrm{AA} + \mathrm{BB}\left(\frac{t-1}{t+1}\right),$$

where we define

$$\mathrm{AA} = \frac{a_1 - \alpha}{\beta}, \qquad \mathrm{BB} = \frac{[(a_1 - \alpha)^2 + a_1\beta^2]^{1/2}}{\beta}. \quad \text{(A9)}$$

We finally arrive at

$$\frac{2\mathrm{BB}}{f_1(g_1)^{1/2}}\int_{t_1}^{t_2}\frac{|t+1|dt}{(t^2+p)(t^2+q)^{1/2}}, \quad \text{(A10)}$$

with

$$p = f_2/f_1, \qquad q = g_2/g_1$$

and

$$f_1 = (\mathrm{AA} + \mathrm{BB})^2 + \beta(\mathrm{AA} + \mathrm{BB}) + \alpha,$$
$$f_2 = (\mathrm{AA} - \mathrm{BB})^2 + \beta(\mathrm{AA} - \mathrm{BB}) + \alpha,$$
$$g_1 = (\mathrm{AA} + \mathrm{BB})^2 + a_1,$$
$$g_2 = (\mathrm{AA} - \mathrm{BB})^2 + a_1 \quad \text{(A11)}$$

Note that $|t+1|$ changes form at $t = -1$.

The integral (A10) is split into two integrals of the form

$$\int_{t_1}^{t_2}\frac{dt}{(t^2+p)(t^2+q)^{1/2}} \quad \text{(A12a)}$$

and

$$\int_{t_1}^{t_2}\frac{tdt}{(t^2+p)(t^2+q)^{1/2}}. \quad \text{(A12b)}$$

The first one is brought to standard form (Gradshteyn and Ryzhik 1965, No. 2.172) by substituting $v = t/(t^2+q)^{1/2}$:

$$\int_{v_1}^{v_2}\frac{dv}{(q-p)v^2 + p}. \quad \text{(A13a)}$$

For the second one, using $u = (t^2+q)^{1/2}$, we obtain

$$\int_{u_1}^{u_2}\frac{du}{u^2 + (p-q)}. \quad \text{(A13b)}$$

In the case $\beta = 0$ (on the major axis) the integral (A8) is already of the form (A12a). Specifically, the maximum rotation curve velocity along the major axis can be easily calculated:

$$V_{\rm mx} = \int_{-\infty}^{\infty}\frac{1}{Al^2 + \xi^2}\frac{\xi v_0\sin i}{(\xi^2 + l^2\sin^2 i)^{1/2}}dl\left(\int_{-\infty}^{\infty}\frac{dl}{Al^2 + \xi^2}\right)^{-1}, \quad \text{(A14)}$$

where we assumed $\xi \gg 1$, and A is as defined in equation (A3). The integral on the left has to be transformed as in (A12a), and both integrals are of standard form. We merely state the result:

$$V_{\rm mx} = (v_0\sin i)\frac{2}{\pi}(1 + c^2\tan^2 i)^{1/2}\tan^{-1}\left(\frac{1}{c\tan i}\right). \quad \text{(A15)}$$

REFERENCES

Babcock, H. W. 1939, *Lick Obs. Bull.*, **192**, 42.
Contopoulos, G. 1956, *Zs. Ap.*, **39**, 126.
de Vaucouleurs, G. 1958, *Ap. J.*, **128**, 465.
Elmegreen, D. M. 1980, *Ap. J. Suppl.*, **43**, 37.
Gallagher, J. S., and Hunter, D. A. 1981, *A.J.*, **86**, 1312.
Gradshteyn, I. S., and Ryzhik, I. M. 1965, in *Table of Integrals, Series, and Products* (New York: Academic), p. 80.
Hodge, P. W. 1980, *A.J.*, **85**, 376.
Hodge, P. W., and Kennicutt, R. C. 1982, *A.J.*, **87**, 264.
Hohl, F., and Zang, T. A. 1979, *A.J.*, **84**, 585.
Kent, S. M. 1983, *Ap. J.*, **266**, 562.
Kormendy, A. 1983, *Ap. J.*, **275**, 529.
Lehmann, E. L. 1975, *Nonparametrics: Statistical Methods Based on Ranks* (New York: McGraw-Hill), pp. 32–40.
Lindblad, B. 1956, *Stockholm Obs. Ann.*, **19**, 1.
McElroy, D. B. 1983, *Ap. J.*, **270**, 485.
Miller, R. H., and Smith, B. F. 1979, *Ap. J.*, **227**, 785.
Pellet, A. 1976, *Astr. Ap.*, **50**, 421.
Peterson, C. J. 1978, *Ap. J.*, **221**, 80.
Richstone, D. O., and Shectman, S. A. 1980, *Ap. J.*, **235**, 30.
Sancisi, R., Allen, R. J., and Sullivan, W. T., III. 1979, *Astr. Ap.*, **78**, 217.
Savage, B. D., and Mathis, J. S. 1979, *Ann. Rev. Astr. Ap.*, **17**, 73.
Schechter, P. L., and Gunn, J. E. 1979, *Ap. J.*, **229**, 484.
Schmidt, M. 1957, *Bull. Astr. Inst. Netherlands*, **14**, 17.
Schwarzschild, M. 1982, *Ap. J.*, **263**, 599.
Sellwood, J. A. 1981, *Astr. Ap.*, **99**, 362.
Stark, A. A. 1977, *Ap. J.*, **213**, 368.

M. Schwarzschild and Edwin L. Turner: Department of Astrophysical Sciences, Princeton University, Peyton Hall, Princeton, NJ 08544

Peter Teuben: Kapteyn Laboratorium, P.O. Box 800, 9700 AV Groningen, The Netherlands